Receding-Horizon Energy-Maximising Optimal Control of Wave Energy Systems Based on Moments

Receding-horizon energy-maximising optimal control of wave energy systems based on moments

Nicolás Faedo[a], Yerai Peña-Sanchez[a] and John V. Ringwood[a]

***Abstract*—In this study, we address the issue of real-time energy-maximising control for wave energy converters (WECs), by proposing a receding-horizon optimal control framework based on the concept of a *moment*. This approach is achieved by extending the so-called *moment-based* framework, recently published in the WEC literature, to effectively solve the associated optimal control problem within a finite time-horizon, allowing for real-time performance, and a straightforward inclusion of the wave excitation force $\mathcal{F}_e$ estimation and forecasting requirements, which are intrinsic to the wave energy control application. We present a case study, based on a CorPower-like device, subject to both state and input constraints. We show that the proposed strategy can perform almost identically to the ideal performance case, where full knowledge of $\mathcal{F}_e$ over the time-horizon is assumed available. Moreover, a sensitivity analysis is provided, addressing the impact of wave excitation force estimation and forecasting errors in the computation of the moment-based control input. Two main conclusions can be drawn from this analysis: Forecasting mismatch has a negligible impact on the overall performance of the strategy, while potential differences arising from estimating $\mathcal{F}_e$, in particular, phase errors, can substantially impact total energy absorption.**

***Index Terms*—Wave energy, WEC, receding-horizon, energy-maximising control, optimal control, moment-domain.**

I. Introduction.

OPTIMAL energy extraction for *wave energy converters* (WECs) has the capabilities of reducing the levelised cost of energy extracted from ocean waves, hence greatly helping in the roadmap towards the commercialisation of WEC technologies [1]. Such an objective is virtually always formulated in terms of an *optimal control problem* (OCP). Not only has this real-time OCP to be solved efficiently in computational terms, but energy-maximisation can *only* be achieved by having full (*instantaneous* and *future*) knowledge of the wave excitation force $\mathcal{F}_e$, *i.e.* the force experienced by the WEC due to incoming waves. Unfortunately, for the WEC case (*i.e.* a moving body), $\mathcal{F}_e$ is, in general, immeasurable. Consequently, unknown-input state estimation strategies are virtually always required to provide *instantaneous* values of $\mathcal{F}_e$ (see [2]). Based on these estimates, a number of forecasting techniques have been proposed to predict *future* wave excitation force within a certain time interval [3]. Naturally, the uncertainty of such a prediction increases with longer time horizons, offering a relatively precise prediction (in realistic sea state conditions) for no more than $3 \sim 10$ [s].

Motivated by both the real-time requirements, and the intrinsic estimation and forecasting needs associated with this OCP, *receding-horizon* approaches to WEC control became popular over the last decade, where a number of solutions emerged, stemming from the basic principles of model predictive control (MPC) [4]. Nevertheless, MPC formulations, which are typically based on zero- or first-order hold discretisations (*i.e.* compactly supported basis functions), have (at least) two main drawbacks. Firstly, the objective function employed departs from pure energy-maximisation, given that the problem (discretised as described above) is inherently non-convex, so that the control objective has to be modified to render the OCP tractable. Secondly, the computational requirements of MPC-based strategies can render this approach unsuitable for real-time control of WECs [4]. Spectral [5] and pseudospectral [6], [7] approaches have been proposed, aiming to solve these issues, in which both the OCP and system variables are discretised using sets of global basis functions. [6] effectively provides a computationally efficient solution, but the OCP is modified (similarly to MPC) to solution existence. In contrast, [5] and [7] provide strategies that both consider a purely energy-maximising objective function, and are appealing from a computational perspective, but the existence of solutions to the OCPs proposed is neither guaranteed nor discussed, so that it is not clear under which conditions these OCPs admit an energy-maximising solution, compromising the feasibility of the corresponding pseudospectral approaches.

Recently, a novel energy-maximising control strategy has been presented in [8], [9]. This formalism is based on the system-theoretic concept of a *moment* [10] and maps the original energy-maximising OCP into a concave quadratic program (QP), systematically guaranteeing a unique global solution for the original energy-maximising control objective, subject to both state and input constraints. Though [8], [9] accomplishes the energy-maximising objective, subject to state and input constraints, the mathematical formalism assumes a sufficiently long time interval, where $\mathcal{F}_e$ is *known* into the future, to solve the OCP, which is limiting in terms of real-time implementation.

This paper directly addresses the issue of real-time energy-maximising control of wave energy converters, including the estimation and forecasting needs associated with the WEC control problem, as detailed in the following. Motivated by the appealing features of the moment-based approach, we propose an extension of the strategy proposed in [8], [9] (which is limited in terms of real-time implementation), by introducing a finite (receding) horizon moment-based OCP framework. In particular, this paper provides the following contributions:

- Unlike [8], [9], which requires full knowledge of the wave excitation force $\mathcal{F}_e$ throughout a sufficiently large

[a]Nicolás Faedo, Yerai Peña-Sanchez John V. Ringwood are with the Centre for Ocean Energy Research, Maynooth University, Maynooth, Ireland nicolas.faedo@mu.ie

time-interval, the representation of $\mathcal{F}_e$ in the *moment-domain* is adapted to finite (short) prediction horizons by an appropriate mathematical definition. To that end, and inspired by the technique employed in [5], we propose the use of a family of *apodisation* mappings [11], which effectively alleviate the effects of 'ignoring' the assumptions on $\mathcal{F}_e$, required in [8], [9].

- Based on the representation of $\mathcal{F}_e$ proposed in the item immediately above, a moment-based receding-horizon real-time controller is proposed. We show that the proposed framework retains the intrinsic computational efficiency, and the uniqueness of the corresponding solution, facilitated through the parameterisation of the corresponding OCP using moments.
- Using the unknown-input estimation strategy presented in [12], and the autoregressive (AR) model of [3], we present performance results, in terms of energy-capture, for a full-scale state-of-the-art heaving CorPower[1]-like device, subject to both state and input constraints.
- Finally, we provide a sensitivity analysis, addressing the impact of estimation and forecasting errors on the computation of the moment-based optimal control input and, hence, on total energy absorption. Using the results of this sensitivity analysis, we give a set of recommendations, related to the design of estimation and forecasting techniques for WEC control applications.

The remainder of this paper is organised as follows. Section II introduces the basics behind moment-based theory, while Section III introduces the energy-maximising problem for WECs, using a receding-horizon approach. Section IV details the receding-horizon moment-based control formulation proposed in this paper, while Section V discusses an application case, including a corresponding sensitivity analysis. Finally, Section VI articulates the main conclusions of this study.

A. Notation and Preliminaries.

Standard notation is considered throughout this study. $\mathbb{R}^+$ ($\mathbb{R}^-$) denotes the set of non-negative (non-positive) real numbers. $\mathbb{C}^0$ denotes the set of pure-imaginary complex numbers, and $\mathbb{C}_{<0}$ denotes the set of complex numbers with negative real part. The symbol 0 stands for any zero element, dimensioned according to the context. The notation $\mathbb{N}_q$ indicates the set of all positive natural numbers up to q, *i.e.* $\mathbb{N}_q = \{1, 2, \ldots, q\}$. The symbol $\mathbb{I}_n$ denotes the identity matrix of the space $\mathbb{C}^{n\times m}$, while the notation $\mathbf{1}_{n\times m}$ is used to denote a $n \times m$ Hadamard identity matrix (*i.e.* a $n \times m$ matrix with all its entries equal to 1). The spectrum of a matrix $A \in \mathbb{R}^{n\times n}$, *i.e.* the set of its eigenvalues, is denoted as $\lambda(A)$. The symbol $\bigoplus$ denotes the direct sum of n matrices, *i.e.* $\bigoplus_{i=1}^{n} A_i = \text{diag}(A_1, A_2, \ldots, A_n)$. The notation $\Re\{z\}$ and $\Im\{z\}$, with $z \in \mathbb{C}$, stands for the *real-part* and the *imaginary-part* operators, respectively. The *Kronecker product* between two matrices $M_1 \in \mathbb{R}^{n\times m}$ and $M_2 \in \mathbb{R}^{p\times q}$ is denoted by $M_1 \otimes M_2 \in \mathbb{R}^{np\times mq}$, while the *Kronecker sum* of two matrices P_1 and P_2, with $P_1 \in \mathbb{R}^{n\times n}$ is denoted as $P_1 \hat{\oplus} P_2$. The convolution between two functions f and g over the set $\Omega \subset \mathbb{R}$, *i.e.* $\int_\Omega f(\tau)g(t-\tau)d\tau$ is denoted as $f * g$. Finally, the symbol $\varepsilon_n \in \mathbb{R}^n$ denotes a vector with odd entries equal to 1 and even entries equal to 0.

[1]The reader is referred to [13] for further detail on the CorPower device.

II. Moment-based theory: Fundamentals.

We provide, in this section, a brief summary of moment-based theory, including the definition of *moments*, for linear systems (see [10]). Consider the dynamical system

$$\dot{x} = Ax + Bu, \quad y = Cx, \tag{1}$$

where $x(t) \in \mathbb{R}^n$, $u(t) \in \mathbb{R}$, $y(t) \in \mathbb{R}$, the triple of (constant) matrices (A, B, C) is dimensioned as $A \in \mathbb{R}^{n\times n}$ and $\{B, C^\intercal\} \subset \mathbb{R}^n$. Assume that system (1) is minimal (*i.e.* controllable and observable). Let the external input u, be written as the output of the so-called *signal generator*:

$$\dot{\xi} = S\xi, \quad u = L\xi, \tag{2}$$

with $\xi(t) \in \mathbb{R}^\nu$, $S \in \mathbb{R}^{\nu\times\nu}$ and $L^\intercal \in \mathbb{R}^\nu$.

Lemma 1. [10] Consider system (1) and the autonomous signal generator (2). Assume that the triple $(L, S, \xi(0))$ is minimal, $\lambda(A) \subset \mathbb{C}_{<0}$, $\lambda(S) \subset \mathbb{C}^0$ and the eigenvalues of S are simple. Then, there is a unique matrix $\underline{Y}^\intercal \in \mathbb{R}^\nu$ such that the steady-state response of the output of the interconnected system (1)-(2) is $y_{\text{ss}}(t) = \underline{Y}\xi(t)$.

Remark 1. The minimality of the triple $(L, S, \xi(0))$ implies the observability of (S, L) and the excitability[2] of $(S, \xi(0))$.

Remark 2. For linear systems excitability is equivalent to reachability, *i.e.* with $\xi(0)$ as the input matrix, see [14].

Definition 1. The matrix $\underline{Y}$ is the *moment* of system (1) at the signal generator (2).

Remark 3. From now on, we refer to the matrix $\underline{Y}$ as the *moment-domain equivalent* of y.

III. Optimal control for WECs.

A. WEC dynamics.

We begin this section by recalling from, for example, [15], some well-known basics behind control-oriented WEC modelling, where we assume a 1-degree-of-freedom (DoF) device, to simplify the notation used throughout this paper[3]. In particular, *linear potential flow theory* is adopted [15], which directly stems from the Navier-Stokes equations, under linear wave theory, and assuming inviscid and incompressible flows.

Remark 4. Note that the modelling assumptions considered herein are consistent (and predominant) across a wide variety of WEC control and estimation applications presented in the literature (see [4]).

The linearised equation of motion of a 1-DoF WEC can be expressed, in the time-domain, as:

$$m\ddot{x} = \mathcal{F}_r + \mathcal{F}_h + \mathcal{F}_e - u, \tag{3}$$

[2]We refer the reader to [14] for further detail on the concept of excitability for a general class of systems.

[3]We note that a similar analysis can be carried out for multi-DoF devices following the moment-based multiple-input, multiple-output framework presented in [9].

with m the mass of the buoy, $x : \mathbb{R}^+ \to \mathbb{R}$ the device excursion (displacement), $\mathcal{F}_e : \mathbb{R}^+ \to \mathbb{R}$ the wave excitation force (external input), $\mathcal{F}_h$ the hydrostatic restoring force, $\mathcal{F}_r$ the radiation force, and $u : \mathbb{R}^+ \to \mathbb{R}$ the exerted power-take off (PTO) control force. The hydrostatic force can be written as $\mathcal{F}_h(t) = -s_h x(t)$, where $s_h = \rho g_r D$ denotes the hydrostatic stiffness, with ρ the water density, D the characteristic area of the device, and g_r the gravitational constant. The radiation force $\mathcal{F}_r$ is modelled using the well-known Cummins' equation [16], can be written as

$$\mathcal{F}_r(t) = -\mu_\infty \ddot{x}(t) - \int_{\mathbb{R}^+} k(\tau)\dot{x}(t-\tau)d\tau, \tag{4}$$

where $\mu_\infty = \lim_{\omega \to +\infty} \tilde{A}(\omega)$, $\mu_\infty > 0$ represents the added-mass at infinite frequency, $\tilde{A}(\omega)$ is the radiation added mass [15], and $k : \mathbb{R}^+ \to \mathbb{R}$ is the (causal) radiation impulse response function, containing the memory effect of the fluid response. Finally, the equation of motion of the WEC[4] is

$$\mathcal{M}\ddot{x} + k * \dot{x} + s_h x = \mathcal{F}_e - u, \tag{5}$$

with $\mathcal{M} = m + \mu_\infty$.

Remark 5. The hydrodynamic characteristics of the WEC device under analysis (including the impulse response mapping k, $\tilde{A}(\omega)$, and μ_∞) can be readily computed using *boundary element method solvers*, such as NEMOH (open source) [17].

B. Energy-maximising control as a finite-horizon OCP.

To appropriately present our moment-based strategy, we first provide a formal definition of the energy-maximising control problem within a receding-horizon framework.

Let the set of state and input (inequality) constraints be:

$$|x(t)| \leq X_{\max}, \quad |\dot{x}(t)| \leq V_{\max}, \quad |u(t)| \leq U_{\max}, \tag{6}$$

with $t \in \mathbb{R}^+$, and where $\{X_{\max}, V_{\max}, U_{\max}\} \subset \mathbb{R}^+$ define the displacement, velocity, and control input limits, respectively. The control objective is to maximise the useful energy absorbed from incoming waves, converted in the PTO system, over a finite-time interval, while consistently respecting physical limits associated with device and actuator dynamics (PTO). This can be written in terms of the following receding-horizon optimal control problem as

$$u_N^{\text{opt}} = \arg\max_{u_N} \frac{1}{T_h} \int_{\Xi_N} u_N(\tau)\dot{x}(\tau)d\tau,$$

subject to:

$$\begin{cases} \text{WEC dynamics (5)}, \\ \text{state and input constraints (6)}, \\ x(t_N^m) = x^m(t_N^m), \\ \dot{x}(t_N^m) = \dot{x}^m(t_N^m), \end{cases} \tag{7}$$

with $T_h \in \mathbb{R}^+$ the *time-horizon*, where we optimise energy-capture within the *time-window* $\Xi_N = [N\Delta_h, N\Delta_h + T_h] \subset \mathbb{R}^+$, $N > 0$ integer, by means of the control input $u_N^{\text{opt}} : \Xi_N \to \mathbb{R}$, and where Δ_h is denoted as the *receding time-step*.

[4]Note that equation (5) describes the motion of *a generic* floating body, under linear potential flow theory.

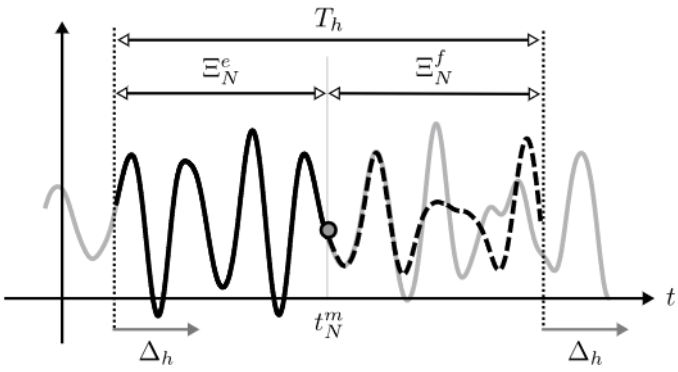

Fig. 1. Sets and time constants involved in the receding-horizon OCP defined in (7). The solid- and dashed-black lines represent *estimated* and *forecasted* values of $\mathcal{F}_e$ (*i.e.*, the approximated excitation force), respectively, while the solid grey line is the target excitation force $\mathcal{F}_e$. The solid-grey circle represents the *current* time instant.

Remark 6. Note that the definition of the time-window Ξ_N is strongly linked to the estimation and forecasting requirements of the wave excitation force (see [18]), and the representation of $\mathcal{F}_e$ in moment-domain (see Section IV).

Following Remark 6, we formally write the set Ξ_N as

$$\begin{aligned} \Xi_N &= [N\Delta_h, t_N^m) \cup t_N^m \cup (t_N^m, N\Delta_h + T_h], \\ &= \Xi_N^e \cup t_N^m \cup \Xi_N^f, \end{aligned} \tag{8}$$

where Ξ_N^e and Ξ_N^f correspond with *past* (estimated) and *future* (forecasted) values of $\mathcal{F}_e$, respectively. The variable $t_N^m \in \Xi_N$ corresponds to the *current* time instant, which (without any loss of generality) is located in the centre of the time-window Ξ_N, *i.e.* $t_N^m = T_h/2 + N\Delta_h$. The distribution of the sets and time constants described above is illustrated in Fig. 1. The additional set of (two) equality constraints in (7) are used to guarantee continuity of the state variables x and $\dot{x}$, under the optimal control action u_N^{opt}, where x^m and $\dot{x}^m$ denote the *measured* values of displacement and velocity, respectively.

We can summarise the receding-horizon OCP of equation (7) in three basic steps[5]:

1) $u_N^{\text{opt}} \leftarrow$ Solve (7) for the time-window Ξ_N.
2) Apply u_N^{opt} in the interval $\Xi_N^u = [N\Delta_h, (N+1)\Delta_h]$.
3) Replace Ξ_N by Ξ_{N+1} accordingly and go back to 1).

IV. Receding-horizon moment-based approach.

Based on the receding-horizon OCP posed in (7), and the theoretical framework developed in [8], [9], we now formally propose a moment-based receding-horizon controller. In particular, Section IV-A discusses the representation of the input $\mathcal{F}_e$ in the moment-domain, for this receding-horizon approach, while Section IV-B effectively proposes an energy-maximising real-time controller for WECs.

A. Input representation in the moment-domain.

Though highly computationally efficient, a standing assumption for the moment-based control strategy presented in [8], [9] is that the wave excitation input $\mathcal{F}_e$ can be

[5]Note that these steps are standard for any receding-horizon technique [4].

characterised by a *periodic* mapping. The following framework aims to alleviate the effect of this assumption.

Remark 7. Note that, if the time-horizon T_h is considered to be sufficiently large, then the signal $\mathcal{F}_e$ can be effectively considered T_h-periodic, for any practical purposes.

Remark 7 itself poses a contradiction: while the moment-based controller [8], [9] would require a sufficiently large time T_h, state-of-the-art forecasting algorithms are not usually able to provide an accurate prediction of $\mathcal{F}_e$ for more than a couple of seconds [12]. In addition, a large T_h can potentially challenge the real-time capabilities of [8], [9].

Motivated by the fact that this periodicity (or sufficiently large T_h) condition is limiting in terms of real-time implementation, we introduce, in this section, a framework to alleviate the effects of this standing assumption. Suppose $\tilde{\mathcal{F}}_{e_N} : \Xi_N \to \mathbb{R}$ denotes the approximated wave excitation input for the time-window Ξ_N, composed of *both* estimated and forecasted values (see Fig. 1). Using the underlying philosophy of the *short-term Fourier transform* (see [11]), we write the *apodised* wave excitation force input as

$$\lfloor \tilde{\mathcal{F}}_{e_N} \rfloor_\vartheta = \vartheta \tilde{\mathcal{F}}_{e_N}, \tag{9}$$

where the *apodisation* mapping $\vartheta : \Xi_N \times \mathbb{R}^+ \to [0\ 1]$ is used to smoothly bring the excitation force signal, defined for a time-horizon T_h, down to zero at the edges of the set Ξ_N. This effectively reduces the spectral leakage produced by the discontinuities arising from truncating the signal $\tilde{\mathcal{F}}_e$ on the (potentially) short time-horizon T_h. In other words, the apodised signal $\lfloor \tilde{\mathcal{F}}_{e_N} \rfloor_\vartheta$ is smoothly brought to zero at the boundaries so that the derivative of its periodic extension is sufficiently smooth. The family of apodisation functions considered herein are the so-called *Planck-taper* mappings [19]. This set of functions was first suggested within the theory of gravitational waves, and stem from the basic functional form of the Planck distribution, *i.e.*

$$\vartheta(t,\gamma) = \begin{cases} \frac{1}{e^{\mathscr{Z}_+(t,\gamma)}+1}, & t_N^i \leq t < \gamma t_N^f, \\ 1, & \gamma t_N^f \leq t < (1-\gamma) t_N^f, \\ \frac{1}{e^{\mathscr{Z}_-(t,\gamma)}+1}, & (1-\gamma) t_N^f \leq t \leq t_N^f, \\ 0, & t < t_N^i \ \vee \ t > t_N^f, \end{cases} \tag{10}$$

where $\{t_N^i, t_N^f\} \subset \Xi_N$ are defined as $t_N^i = N\Delta_h$ and $t_N^f = N\Delta_h + T_h$, and the mapping $\mathscr{Z}$ is such that

$$\mathscr{Z}_\pm(t,\gamma) = \frac{2\gamma}{1 \pm \left(\frac{2\gamma}{t_N^f} - 1\right)} + \frac{2\gamma}{1 - 2\gamma \pm \left(\frac{2\gamma}{t_N^f} - 1\right)}. \tag{11}$$

An example, showing both $\tilde{\mathcal{F}}_e$ and $\lfloor \tilde{\mathcal{F}}_{e_N} \rfloor_\vartheta$ for a time-window Ξ_N and parameter $\gamma = 0.5$, is shown in Fig. 2.

Remark 8. The selection of the set of apodisation functions (10) is motivated by its intrinsic optimality with respect to the preservation of the power spectrum of the wave excitation input (see [19]), being the latter a key variable in the OCP (7). Nevertheless, different apodisation functions[6] can be considered straightforwardly, without further modifications.

[6]The reader is referred to [11] for further detail on different apodisation mappings.

Let $\omega_0 \in \mathbb{R}^+$ be the *fundamental frequency* for the time-horizon T_h, *i.e.* $\omega_0 = 2\pi/T_h$. Following the theoretical framework proposed in [8], [9], both the apodised wave excitation force $\lfloor \tilde{\mathcal{F}}_{e_N} \rfloor_\vartheta$ and control input u are expressed in terms of a *signal generator* described by the set of equations

$$\dot{\xi} = S\xi, \quad \lfloor \tilde{\mathcal{F}}_{e_N} \rfloor_\vartheta = L_{e_N}\xi, \quad u_N = L_{u_N}\xi, \tag{12}$$

where $\xi(t) \in \mathbb{R}^\nu$, $\{L_{u_N}^\intercal, L_{e_N}^\intercal\} \subset \mathbb{R}^\nu$ and the dynamic matrix $S \in \mathbb{R}^{\nu\times\nu}$ can be written in block-diagonal form as

$$S = \bigoplus_{p=1}^{f} \begin{bmatrix} 0 & p\omega_0 \\ -p\omega_0 & 0 \end{bmatrix}, \tag{13}$$

while $\nu = 2f$, $f > 0$ integer. The initial condition is set to $\xi(0) = \varepsilon_\nu$ and the pair $(S, L_{e_N} - L_{u_N})$ is assumed observable.

Remark 9. $\lambda(S) = \{\pm jp\omega_0\}_{p=1}^f$ in (12), *i.e.* the apodised excitation force is assumed to be a T_h-periodic mapping, composed of a finite number f of harmonics of the fundamental frequency ω_0. In particular, the maximum frequency used to describe the apodised excitation force, *i.e.* the so-called cut-off frequency ω_c, is simply given as $\omega_c = f\omega_0$.

The excitation force input vector L_{e_N}, for a particular time-window Ξ_N, can be straightforwardly obtained using a least-squares approach: Let $\mathcal{T}_\xi = \{t_i\}_{i=1}^P \subset \Xi_N$ be a finite set of $P > \nu$ (integer) uniformly-spaced time instants, and let $\Lambda_{\mathcal{T}_\xi} \in \mathbb{R}^{\nu\times P}$ and $\Lambda^\intercal_{\lfloor \tilde{\mathcal{F}}_{e_N} \rfloor_\vartheta} \in \mathbb{R}^P$ be defined as

$$\begin{aligned} \Lambda_{\mathcal{T}_\xi} &= \begin{bmatrix} \xi(t_1) & \dots & \xi(t_P) \end{bmatrix}, \\ \Lambda_{\lfloor \tilde{\mathcal{F}}_{e_N} \rfloor_\vartheta} &= \begin{bmatrix} \lfloor \tilde{\mathcal{F}}_{e_N} \rfloor_\vartheta(t_1) & \dots & \lfloor \tilde{\mathcal{F}}_{e_N} \rfloor_\vartheta(t_P) \end{bmatrix}. \end{aligned} \tag{14}$$

Then, we define L_{e_N} using the following expression:

$$L_{e_N} := \Lambda_{\lfloor \tilde{\mathcal{F}}_{e_N} \rfloor_\vartheta} \Lambda_{\mathcal{T}_\xi}^\intercal (\Lambda_{\mathcal{T}_\xi} \Lambda_{\mathcal{T}_\xi}^\intercal)^{-1}, \tag{15}$$

where the invertibility of the matrix $\Lambda_{\mathcal{T}_\xi}\Lambda_{\mathcal{T}_\xi}^\intercal$ is guaranteed by the excitability of the pair (S, ε_ν), see [14].

Remark 10. Though real-time performance is already available with (15) (see Section V), we note that, if required, extra computational speed could be achieved using a *recursive* least-squares implementation instead of (15).

B. Receding-horizon moment-based controller.

Analogously to [8], [9], we can equivalently write the WEC dynamics, expressed in (5), as

$$\dot{\varphi} = A\varphi - B(k * C\varphi) + B(\mathcal{F}_e - u), \quad y = C\varphi, \tag{16}$$

where $\varphi(t) = [\varphi_1(t), \varphi_2(t)]^\intercal = [x(t), \dot{x}(t)]^\intercal \in \mathbb{R}^2$, is the state-vector of the continuous-time model and $y = \dot{x}$ is the output of the system (assuming velocity to be the measurable device output). Using this representation, the triple of matrices (A, B, C) parameterising equation (16), is given by

$$A = \begin{bmatrix} 0 & 1 \\ -s_h\mathcal{M}^{-1} & 0 \end{bmatrix}, B = \begin{bmatrix} 0 \\ \mathcal{M}^{-1} \end{bmatrix}, C^\intercal = \begin{bmatrix} 0 \\ 1 \end{bmatrix}. \tag{17}$$

Based on the moment-domain representation of the (apodised) wave excitation force (see Section IV-A), and the

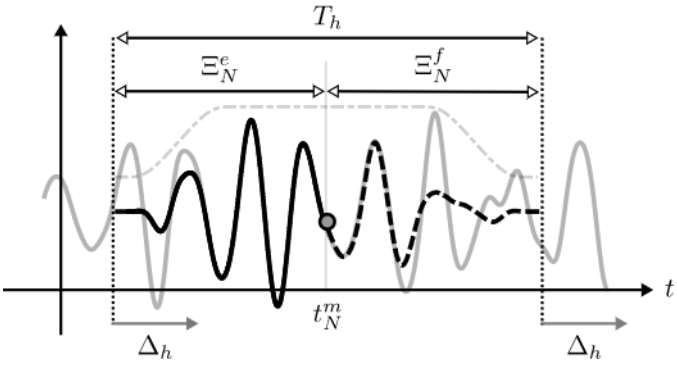

Fig. 2. Target estimation force $\mathcal{F}_{e_N}$ (solid grey), and the (apodised) approximated excitation force $\lfloor \tilde{\mathcal{F}}_{e_N} \rfloor_\vartheta = L_{e_N}\xi$ (black), with L_{e_N} as in (15), for the time-window Ξ_N. The apodisation mapping ϑ is plotted with a dash-dotted grey line, while the solid-grey circle represents the *current* time.

equation of motion (16), we now propose a receding-horizon moment-based energy-maximising controller subject to state and input constraints. In particular, under this moment-based framework (and following [8], [9]), the steady-state output response of system (16) can be computed as (see Lemma 1)

$$y = \underline{Y}\xi, \qquad \underline{Y} = (L_{e_N} - L_{u_N})\Phi_\varphi^{\mathscr{R}}, \tag{18}$$

where $\underline{Y}$ is the moment-domain equivalent of the velocity of the device (*i.e.* the output y in (16)), and where the matrix $\Phi_\varphi^{\mathscr{R}} \in \mathbb{R}^{\nu\times\nu}$, depending on the system dynamics defined in (16), is defined as

$$\begin{aligned} \Phi_\varphi^{\mathscr{R}} &= (\mathbb{I}_\nu \otimes C)\Phi_\varphi^{-1}(\mathbb{I}_\nu \otimes -B), \\ \Phi_\varphi &= \big(S \hat{\oplus} A\big) + \mathscr{R}^\intercal \otimes -BC. \end{aligned} \tag{19}$$

Finally, the matrix $\mathscr{R}$, representing the moment-domain equivalent of the radiation force term in (16), is given by

$$\mathscr{R} = \bigoplus_{p=1}^{f} \begin{bmatrix} \Re\{K(jp\omega_0)\} & \Im\{K(jp\omega_0)\} \\ -\Im\{K(jp\omega_0)\} & \Re\{K(jp\omega_0)\} \end{bmatrix}, \tag{20}$$

with $K : \mathbb{C}^0 \to \mathbb{C}$ the frequency-response mapping associated with the radiation impulse response function k.

Let $\mathcal{T}_\rho = \{t_i\}_{t=1}^{N_\rho} \subset \Xi_N$ be a set of uniformly-distributed time-instants[7] (*collocation points*), and define $\Lambda \in \mathbb{R}^{\nu\times N_\rho}$ and $\Delta \in \mathbb{R}^{\nu\times 2N_\rho}$ as

$$\Lambda = \begin{bmatrix} \xi(t_1) & \dots & \xi(t_{N_\rho}) \end{bmatrix}, \quad \Delta = \begin{bmatrix} \Lambda & -\Lambda \end{bmatrix}. \tag{21}$$

With the definition of Λ and Δ in (21), and introducing the moment-domain equivalent of the velocity (18) in the objective function (7), we can write the moment-based control input u_N^{opt}, for a given time window Ξ_N, as $u_N^{\text{opt}} = L_{u_N}^{\text{opt}}\xi$, where the vector $L_{u_N}^{\text{opt}}$ is the unique global maximiser of the concave QP (see [8], [9]):

$$L_{u_N}^{\text{opt}} = \arg\max_{L_{u_N}^\intercal \in \mathbb{R}^\nu} -\frac{1}{2}\, L_{u_N}\Phi_\varphi^{\mathscr{R}^\intercal} L_{u_N}^\intercal + \frac{1}{2}\, L_{e_N}\Phi_\varphi^{\mathscr{R}^\intercal} L_{u_N}^\intercal$$

subject to:

$$\begin{aligned} &L_{u_N}\mathcal{A}_x \le \mathcal{B}_x, \qquad L_{u_N}\mathcal{A}_{\dot{x}} \le \mathcal{B}_{\dot{x}}, \qquad L_{u_N}\mathcal{A}_u \le \mathcal{B}_u, \\ &L_{u_N}\mathcal{A}_x^{\text{eq}} = \mathcal{B}_x^{\text{eq}}, \qquad L_{u_N}\mathcal{A}_{\dot{x}}^{\text{eq}} = \mathcal{B}_{\dot{x}}^{\text{eq}}, \end{aligned} \tag{22}$$

[7]See [8], [9] for a discussion on the selection of the set $\mathcal{T}_\rho$.

where the pairs of matrices $(\mathcal{A}_x, \mathcal{B}_x)$, $(\mathcal{A}_{\dot{x}}, \mathcal{B}_{\dot{x}})$ and $(\mathcal{A}_u, \mathcal{B}_u)$ are associated with the state and input inequality constraints in (6) on displacement, velocity and control (PTO) input, respectively. In contrast to [8], [9], we now include the pairs of matrices $(\mathcal{A}_x^{\text{eq}}, \mathcal{B}_x^{\text{eq}})$ and $(\mathcal{A}_{\dot{x}}^{\text{eq}}, \mathcal{B}_{\dot{x}}^{\text{eq}})$ to fulfill the equality constraints in (7) at each current time instant, *i.e.* at $t = t_N^m \in \Xi_N$. In particular, the explicit expressions for the pairs of matrices involved in (22) are given by

$$\begin{aligned} \mathcal{A}_x &= -\Phi_\varphi^{\mathscr{R}^\intercal} S^{-1}\Delta, & \mathcal{B}_x &= X_{\max}\mathbf{1}_{2N_\rho}^\intercal + L_{e_N}\mathcal{A}_x, \\ \mathcal{A}_{\dot{x}} &= -\Phi_\varphi^{\mathscr{R}^\intercal}\Delta, & \mathcal{B}_{\dot{x}} &= V_{\max}\mathbf{1}_{2N_\rho}^\intercal + L_{e_N}\mathcal{A}_{\dot{x}}, \\ \mathcal{A}_u &= \Delta, & \mathcal{B}_u &= U_{\max}\mathbf{1}_{2N_\rho}^\intercal, \\ \mathcal{A}_x^{\text{eq}} &= -\Phi_\varphi^{\mathscr{R}^\intercal} S^{-1}\xi(t_N^m), & \mathcal{B}_x^{\text{eq}} &= x^m(t_N^m) + L_{e_N}\mathcal{A}_x^{\text{eq}}, \\ \mathcal{A}_{\dot{x}}^{\text{eq}} &= -\Phi_\varphi^{\mathscr{R}^\intercal}\xi(t_N^m), & \mathcal{B}_{\dot{x}}^{\text{eq}} &= \dot{x}^m(t_N^m) + L_{e_N}\mathcal{A}_{\dot{x}}^{\text{eq}}, \end{aligned} \tag{23}$$

Remark 11. Following the receding-horizon approach to WEC control discussed in Section III-B, the moment-based optimal control problem, proposed in (22), is solved for a particular time window Ξ_N, and then applied to the system for the time interval $\Xi_N^u = [N\Delta_h, (N+1)\Delta_h]$, *i.e.* for a single receding time-step Δ_h. The time window is then subsequently shifted, *i.e.* $\Xi_N \mapsto \Xi_{N+1}$, and the process is repeated.

V. Case study.

To demonstrate the performance of the receding-horizon moment-based controller proposed in Section IV, we consider a full-scale state-of-the-art CorPower-like wave energy device, oscillating in heave (translational motion). Fig. 3 presents a schematic illustration of the CorPower-like WEC, along with its corresponding hydrodynamic characterisation[8], *i.e.* the frequency-response $K(j\omega)$ associated with the impulse response mapping k. The dimensions of this device are based on the experimental study performed in [13].

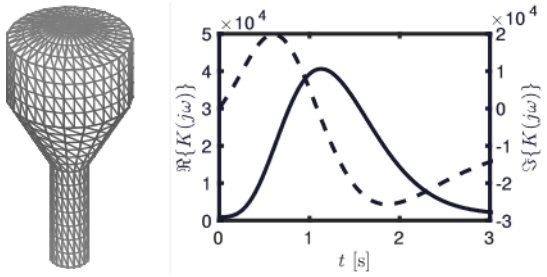

Fig. 3. Schematic of the CorPower-like device, along with the frequency-response of the radiation impulse response mapping k.

In the remainder of this section, we consider waves generated stochastically from a JONSWAP spectrum [20], with a fixed significant wave height H_s of 2 [m], peak period $T_p \in [5, 12]$ [s] and peak shape parameter $\gamma = 3.3$. Since the waves are generated from sets of random amplitudes [21], it is found that a mean of ≈ 40 simulations (per sea state) is necessary to obtain statistically consistent performance results for the controller presented in this study.

[8]$K(j\omega)$ has been computed using NEMOH (see Remark 5).

Remark 12 (On the selection of T_h). The time-horizon T_h, which characterises the time-window Ξ_N, has to be selected bearing in mind the following trade-off. While a larger T_h (*i.e.* a smaller fundamental frequency ω_0) implies a more refined description of the apodised excitation input, with respect to the least-squares procedure described in (15) (see Remark 9), an increased number of harmonics f is required to reach a given cut-off frequency ω_c, which naturally increases the computational requirements of the strategy (note that the order of the matrices involved in the QP problem (22) directly depends on f). This trade-off can be simply assessed by means of numerical analysis.

For this case study, and following Remark 12, the time-horizon is selected as $T_h = 60$ [s], i.e. we consider 30 [s] of both estimated and forecasted values of $\mathcal{F}_e$. This corresponds to a fundamental frequency $\omega_0 = 2\pi/60$ [rad/s], which provides accurate results with respect to the least-square procedure described in (15), with mild computational requirements. The receding time-step is fixed as $\Delta_h = 0.1$ [s], while the dimension (order) of the signal generator (12) is chosen as $\nu = 60$ (corresponding with a cut-off frequency of $\omega_c \approx 6$ [rad/s]). With respect to state constraints, we fix the maximum allowed displacement and velocity values as $X_{\text{max}} = 2$ [m] and $V_{\text{max}} = 2$ [m/s], respectively.

Remark 13. We note that the moment-based controller runtime, *i.e.* the time required to compute the energy-maximising optimal control input for the duration of the receding-step Δ_h, is in the order of ~ 1 [ms] $\ll \Delta_h$ for the totality of the preceding simulations (implemented in MATLAB), hence always easily achieving real-time performance. Naturally, the speed at which computations are performed can be further improved (if required) by simply implementing this algorithm in a compiled language, such as C or C++.

As discussed in Section I, the unknown-input estimation strategy, selected to compute the estimation section of $\tilde{\mathcal{F}}_{e_N}$, for each time-window Ξ_N^e, is based on a combination of Kalman filtering and the internal model principle of control theory, as presented (and tuned) in [12]. The forecasting algorithm considered, over the set Ξ_N^f, is the AR model proposed in [3], where the order $\mathcal{O}$ is set to 200 (see Section V-C).

A. Results and discussion.

Initial controller performance assessment focusses on energy absorption under both displacement and velocity constraints. Fig. 4 shows absorbed energy for sea states with $H_s = 2$ [m] and $T_p \in [5, 12]$, where the displacement and velocity of the CorPower-like device are constrained to X_{max} and V_{max}, respectively. The solid-black line represents the *ideal* (performance) scenario, where the excitation force is assumed to be *perfectly* known over each time-window, *i.e.* $\mathcal{F}_{e_N} = \tilde{\mathcal{F}}_{e_N}$, $\forall N$, while the dotted-grey line shows the *actual* performance of the moment-based controller, where we utilise the *approximated* excitation force $\tilde{\mathcal{F}}_{e_N}$, computed with both estimation and forecasting algorithms. Clearly, the *actual* performance of the proposed receding-horizon moment-based approach is almost indistinguishable from its ideal counterpart, being able to perform optimally, with differences of less than 5% in terms of energy absorption. Figure 4 also includes absorbed energy obtained with a reactive (displacement and velocity) feedback, used here as benchmark strategy (see [15]).The feedback gain is computed using exhaustive search, ensuring that the specified constraints are met for each sea-state analysed (as in, for instance, [22]). Note that the receding-horizon moment-based strategy is consistently outperforming the feedback controller in terms of energy-absorption, for the totality of the sea states.

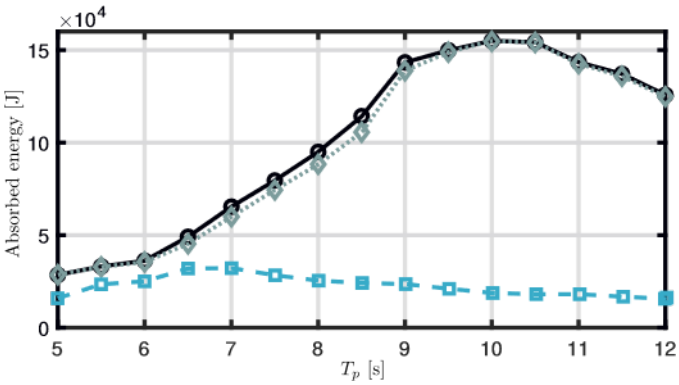

Fig. 4. Constrained (displacement and velocity) energy absorption for the receding-horizon moment-based energy-maximising controller proposed in this paper. The solid-black and dotted-grey lines represent the *ideal* and *actual* performance results, respectively. The dashed-cyan line indicates performance obtained with a reactive feedback controller.

To fully illustrate the capabilities of the proposed strategy, Fig. 5 presents time traces of displacement (**a**, left axis, solid-black), velocity (**a**, left axis, dashed-black) and control input (**b**, left axis, solid-black), for a specific sea-state realisation with $T_p = 8$ [s], where we also include a maximum control (PTO) force constraint $U_{\text{max}} = 1 \times 10^6$ [N]. We note that some key features can be directly appreciated from Fig. 5, which we discuss in the following. To begin with, the state and input limits, under the action of the receding-horizon moment-based control strategy, are being consistently respected $\forall t$, hence illustrating the capability of the approach to maximise energy absorption for WECs, while respecting the physical limitations of both device and actuator (PTO). Moreover, we note that, even in this fully constrained case, the velocity of the device under optimal control conditions remains 'in-phase'[9] with $\mathcal{F}_e$ (right axis, dotted-gray), agreeing with well-known theoretical results for unconstrained energy-maximisation of WECs [15].

B. Sensitivity analysis: Estimation.

We now present a sensitivity analysis for the proposed receding-horizon moment-based controller, concerning errors in the *estimated* wave excitation force, over the time-interval Ξ_N^e. From now on, aiming to simplify the presentation of results, we fix the wave peak period to $T_p = 8$ [s], given that almost identical conclusions can be drawn using different values for $T_p \in [5, 12]$.

[9]We use the term 'in-phase'to indicate that the peaks (local maxima and minima) of both signals are aligned in time.

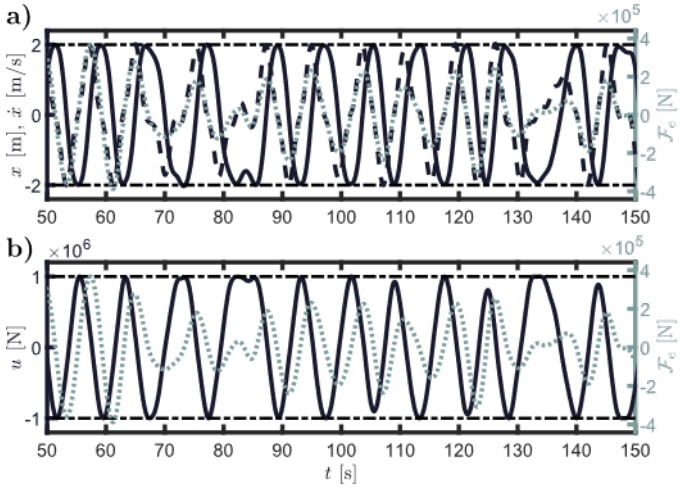

Fig. 5. Motion and control results for wave excitation with $H_s = 2$ [m] and $T_p = 8$ [s]. Plot **a** shows displacement (left axis, solid-black), velocity (left axis, dashed-black), and wave excitation force input (right axis, dotted-grey), while plot **b** presents the corresponding control input (left axis, solid-black), used to elicit the motion results. The dash-dotted horizontal lines represent constraint values.

As discussed in the comparison study [2], there are two main sources of errors affecting $\tilde{\mathcal{F}}_{e_N}$, arising from improper tuning of any unknown-input estimator: Constant errors in instantaneous amplitude (*i.e.* constant deviations in envelope), and instantaneous phase (*i.e.* time-delays). We represent these imperfections within the estimation stage using the criterion specified in what follows.

Remark 14. Another possible error source is the presence of measurement noise, *i.e.* the estimator is tuned in such a way that high frequency noise (affecting motion sensors) is *not* filtered. This effect is not analysed herein: Note that the moment-based representation for the input (discussed in Section IV-A) can intrinsically filter high frequency components, via a suitable selection of ν in (13).

Let $\{F_\alpha, F_\phi\} \subset \Omega_{\text{F}}$, with $\Omega_{\text{F}} = [0.75, 1.25]$, be (error) factors associated with[10] amplitude (**A**) and phase (**P**) of $\tilde{\mathcal{F}}_{e_N}$. We analyse, for $t \in \Xi^e_N$, the following error sources:

$$\begin{aligned} \textbf{A}&: \tilde{\mathcal{F}}_{e_N}(t) \mapsto F_\alpha \tilde{\mathcal{F}}_{e_N}(t), \\ \textbf{P}&: \tilde{\mathcal{F}}_{e_N}(t) \mapsto \tilde{\mathcal{F}}_{e_N}(t + (F_\phi - 1)T_p). \\ \textbf{A+P}&: \tilde{\mathcal{F}}_{e_N}(t) \mapsto F_\alpha \tilde{\mathcal{F}}_{e_N}(t + (F_\phi - 1)T_p). \end{aligned} \tag{24}$$

Case **A** assumes that the amplitude of the estimated signal is not estimated correctly, *i.e.* $\tilde{\mathcal{F}}_e$ is multiplied by a factor F_α, while case **P** effectively considers the existence of a time (phase) delay (positive or negative) between estimated and true excitation force, proportional to the peak period T_p. Lastly, case **A+P** combines both sources of error, by assuming that the estimated excitation force has both amplitude and phase errors, for all possible combinations of $\{F_\alpha, F_\phi\}$ in $[0.75, 1.25]$.

Remark 15. Due to the underlying linearity of the AR model considered in this study, if $\tilde{\mathcal{F}}_{e_N}$ is modified either by scaling, shifting in time, or superposing both cases, for $t \in \Xi^e_N$, this modification propagates within the forecasted time-window Ξ^f_N in the *exact* same manner. In other words, the sources of estimation error described in cases **A**, **P** and **A+P** affect the forecasted signal in the exact same proportions.

Fig. 6 presents an illustrative example of an excitation force signal affected by cases **A** and **P**, for a time-window Ξ_N. In particular, we show the estimated and forecasted excitation force with $F_\alpha = F_\phi = 1$, *i.e.* error-free (solid-black), and for various values of F_α (**a**, green) and F_ϕ (**b**, green).

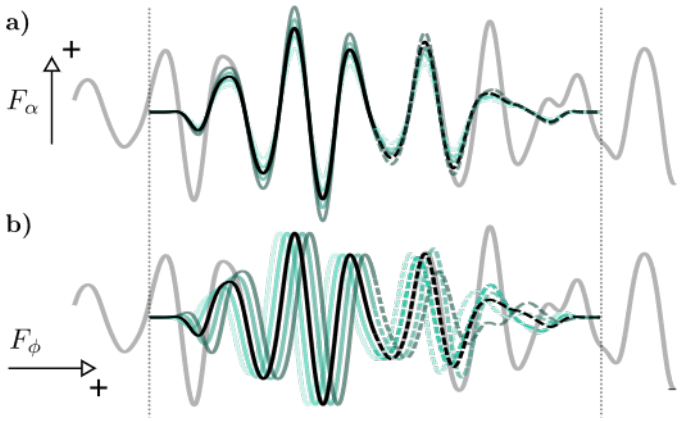

Fig. 6. Illustrative example of cases **A** (**a**, green) and **P** (**b**, green), for a particular estimated (apodised) excitation force signal $\lfloor \tilde{\mathcal{F}}_{e_N} \rfloor_\vartheta$ (solid-black). The target excitation force $\mathcal{F}_e$ is depicted with a solid-grey line.

Taking into account the cases defined in (24), the sensitivity analysis with respect to estimation errors is defined in terms of a suitable performance indicator $R^e_{\mathcal{J}}$. In particular, we define $R^e_{\mathcal{J}}$ as $R^e_{\mathcal{J}}(F_\alpha, F_\phi) = \mathcal{J}(F_\alpha, F_\phi)/\mathcal{J}(1,1)$, where the image of the mapping $\mathcal{J} : \Omega_{\text{F}} \times \Omega_{\text{F}} \to \mathbb{R}$ is the absorbed energy throughout the complete simulation time, for any pair of values (F_α, F_ϕ), under controlled conditions.

Remark 16. To be precise, $R^e_{\mathcal{J}}$ is the ratio between the absorbed energy under the moment-based control strategy (22), *with* and *without* the presence of estimation errors. In other words, the performance indicator $R^e_{\mathcal{J}}$ describes how optimal energy absorption is affected if the unknown-input estimator is not perfectly tuned, distinguishing explicitly between amplitude and phase errors.

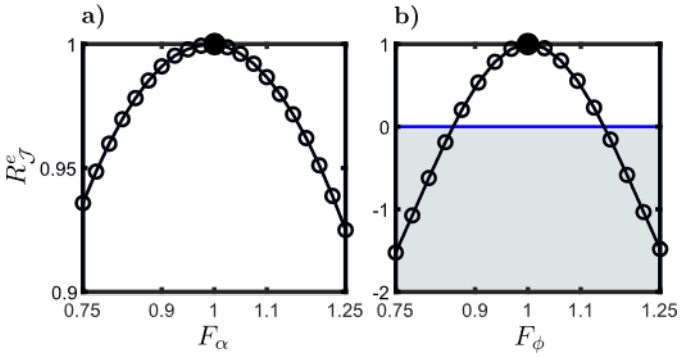

Fig. 7. $R^e_{\mathcal{J}}$ for cases **A** (**a**) and **P** (**b**). A value of $R^e_{\mathcal{J}}$ below zero (solid-blue line) indicates negative energy absorption. The filled black circle indicates absorption with $F_\alpha = F_\phi = 1$.

[10]From now on, we refer to *instantaneous amplitude* and *instantaneous phase* simply as *amplitude* and *phase*, respectively.

Fig. 7 shows performance results for cases **A** (**a**) and **P** (**b**), in terms of $R^e_{\mathcal{J}}(F_\alpha, 1)$ and $R^e_{\mathcal{J}}(1, F_\phi)$, respectively. For case **A**, it can be appreciated that, even under an amplitude deviation of $\pm 25\%$ from its true value, the absorbed energy always remains above 90% of its optimal achievable performance (computed without any estimation amplitude or phase errors). In other words, deviations in amplitude, for the estimated wave excitation force, generate only small deviations in absorbed energy under controlled conditions. This is clearly not the case for phase deviations, *i.e.* case **P**, where a delay (positive or negative) of $\approx$10% of the peak period (around 0.8 [s], for this case study), not only dramatically affects optimal energy absorption, but actually generates negative power (the device starts to drain energy from the electric grid). This clearly indicates that maximal effort should be put into tuning the estimator to guarantee *phase* synchronisation with the target wave excitation signal, hence achieving optimal energy-maximisation, under controlled conditions.

Finally, Fig. 8 shows results for case **A+P**, where both errors in amplitude and phase are analysed simultaneously. Similarly to case **P**, it is clear that the presence of a time-delay (positive or negative) has a much greater impact on energy absorption than any existing differences in estimated amplitude. Interestingly, while positive or negative delays have an almost symmetric effect, underprediction of the wave excitation force amplitude has a lesser impact on performance than overprediction. Note that this behaviour is consistent with that of Fig. 7 (**a**).

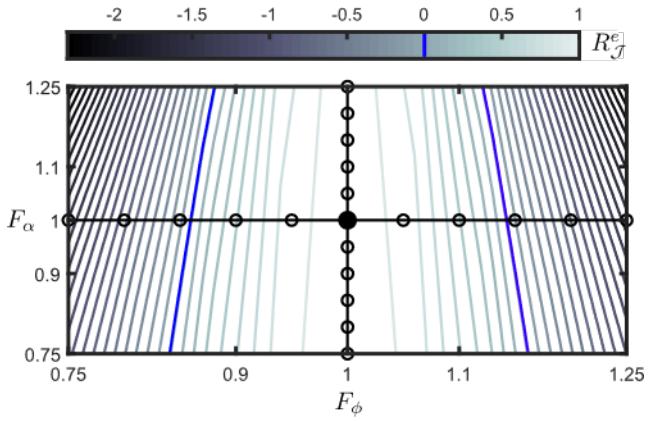

Fig. 8. $R^e_{\mathcal{J}}$ for case **A + P**. A value of $R^e_{\mathcal{J}}$ below zero (solid-blue line) indicates negative energy absorption. Cases **A** and **B** are depicted with solid-black (empty circle) lines. The filled black circle indicates absorption with $F_\alpha = F_\phi = 1$.

C. Sensitivity analysis: Forecasting.

We now consider errors arising purely from the forecasting procedure, *i.e.* we assume that the unknown-input estimator is well-tuned (achieving convergence towards the target excitation force), and that any potential mismatch is only present within the forecasted window Ξ^f_N. To that end, we define the performance indicator $R^f_{\mathcal{J}}(t^f) = \mathcal{J}(t^f)/\mathcal{J}(5)$, where the image of the operator $\mathcal{J} : \mathbb{R}^+ \to \mathbb{R}$ is the energy absorbed, assuming $t^f < 5$ seconds of forecast within 99% and 100% of accuracy.

Remark 17. $R^f_{\mathcal{J}}$ is the ratio of absorbed energy, under controlled conditions, between energy extraction assuming quasi-perfect knowledge of the forecasted signal for a section of Ξ^f_N, and the maximum time-length with achievable forecast with more than 99% of accuracy, *i.e.* $\approx$ 5 [s], obtained from a sufficiently large AR model order $\mathcal{O}$ (here chosen as $\mathcal{O} = 200$). In other words, $R^f_{\mathcal{J}}$ describes how optimal energy absorption is affected in terms of the accuracy of the forecasting algorithm.

Fig. 9 presents performance results in terms of the indicator $R^f_{\mathcal{J}}(t^f)$, while Fig. 10 presents an illustrative example of a forecasted excitation force signal with $t^f = 5$ [s] (dashed-black), and for $t^f < 5$ (dashed-green).

Unlike the *estimation* case discussed in Section V-B, where deviations from the target excitation force can effectively generate negative power absorption, the impact of *forecasting* errors, for the moment-based controller presented in this paper, is almost negligible. Even with $t^f \approx 1$ [s], the controller is able to perform within 99% of its optimal performance, *i.e.* the performance obtained with an AR model with a sufficiently large order.

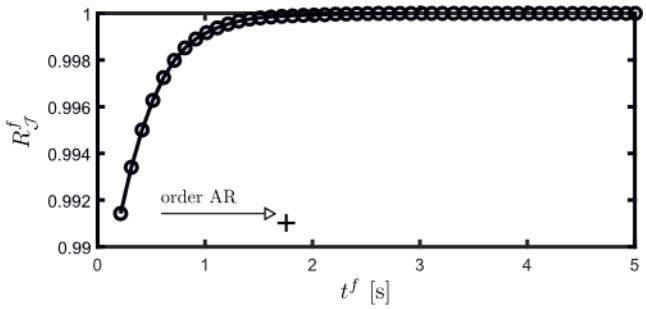

Fig. 9. Sensitivity analysis with respect to forecasting errors in terms of the performance indicator $R^f_{\mathcal{J}}$.

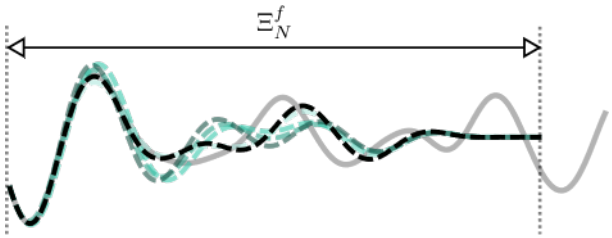

Fig. 10. Illustrative example of a forecasted (apodised) excitation force signal with $t^f = 5$ [s] (dashed-black), and for $t^f < 5$ [s] (dashed-green). The target excitation force $\mathcal{F}_e$ is depicted with a solid-grey line.

VI. Conclusions.

This paper proposes a real-time receding-horizon energy-maximising controller based on moments, by formally extending [8], [9] to a finite-horizon OCP. The representation of the wave excitation force input, in the moment-domain, is adapted to short prediction horizons by the use of a convenient family of apodisation mappings. The optimal control objective is modified accordingly, using a receding-horizon approach, while retaining the intrinsic computational efficiency and